ELSEVIER

Ceramics International 30 (2004) 2241–2246

CERAMICS INTERNATIONAL

www.elsevier.com/locate/ceramint

# Structural characterization of Bi–Zn–Nb–O cubic pyrochlores

Yi Hu [a,*], C.-L. Huang [b]

[a] *Department of Materials Engineering, Tatung University, 40 Chungshan North Road, Taipei, Taiwan, ROC*
[b] *Metal Industries Research & Development Centre, Kaohsiun, Taiwan, ROC*

Received 29 September 2003; received in revised form 30 October 2003; accepted 19 December 2003
Available online 21 April 2004

**Abstract**

Structure and dielectric properties of oxide dielectrics with the composition of $Bi_{1.5}Zn_NNb_{2.5-N}O_{8.5-1.5N}$ (with $N = 0.73$ to 1.20) have been studied. These samples were treated at 1050 °C for 4 h. The cubic pyrochlore phase was found to be predominant as from X-ray diffraction and Raman spectra analysis. Lattice constant of the cubic pyrochlore and dielectric constant of the sample have been found to increase with the increase of Zn content. A model of the structural defects has been proposed to explain the stabilization of the pyrochlore structure. The limitation of composition for the formation of single cubic pyrochlore phase has been attributed to the distribution of oxygen defects.


*Keywords:* B. Defects; Cubic pyrochlore; Oxide ceramics; Dielectric

## 1. Introduction

$Bi_2O_3$–ZnO–$Nb_2O_5$ (BZN) based dielectric ceramics have recently found to be of interest for low-fired high frequency dielectric applications [1–5]. The low sintering temperatures of BZN make them promising candidates for decoupling capacitors in low temperature co-fired ceramic (LTCC) packages. In the BZN system, the cubic pyrochlore structure has been observed to be the predominant phase which forms even with considerable variation in composition [2]. In addition, the dielectric properties of BZN ceramics with cubic pyrochlore phase strongly depend on the composition and heating conditions.

It is well known that perfect cubic pyrochlore oxides are with two different types of oxygen ions with general formula of $A_2B_2O_6O'$ (space group Fd3m, $Z = 8$) [6]. The A ion is coordinated to eight oxygen atoms and the B ion is coordinated to six oxygen atoms. In the bismuth based oxides, $(Bi_{1.5}Zn_{0.5})(Zn_{0.5}Nb_{1.5})O_7$ was claimed to exhibit a cubic pyrochlore structure with the Zn ions occupying both A and B sites [5]. Since the radius of $Zn^{2+}$ (~0.90 Å) is much less than that of $Bi^{3+}$ (~1.17 Å) with eight coordination, the stability of the pyrochlore structure seems to be limited in composition [2,7] and the presence of rather small Zn ions on the eightfold coordinated A sites remained controversial [8,9].

However, structural defects such as oxygen vacancy can form in the BZN ceramics due to the valence compensation for the nonstoichiometric compositions. The accurate structure information is now available for a number of nonstoichiometric pyrochlore oxides with oxygen vacancies [10–12]. Oxygen vacancy in BZN oxides forms when excess Zn ions occupy the B sites. Therefore, it becomes very interesting to study the dielectric properties of the pyrochlore BZN ceramics of the compositions with excess Zn ions.

In this paper, the results of studies on the phase structure and dielectric properties of $Bi_{1.5}Zn_NNb_{2.5-N}O_{8.5-1.5N}$ (with $N = 0.73$ to 1.20) were reported. The nominal compositions of the BZN ceramics were prepared with the variation of Zn/Nb ratio.

## 2. Experimental

The samples with chemical formula of $Bi_{1.5}Zn_NNb_{2.5-N}O_{8.5-1.5N}$ (with $N = 0.73$ to 1.20) were prepared by conventional solid state reaction of the oxides. The raw oxides are reagent grade $Bi_2O_3$ (99.9%), $Nb_2O_5$ (99.9%,), ZnO (99.8%) from STREM Chemicals, Inc., USA. The oxide powders were measured in the appropriate ratios and mixed in de-ionized water using $ZrO_2$ balls in polyethylene containers for 4 h. The mixture was dried in an oven

* Corresponding author. Tel.: +886-2-2592-5252; fax: +886-2-2593-6897.
*E-mail address:* huyi@ttu.edu.tw (Y. Hu).

0272-8842/$30.00 
doi:10.1016/j.ceramint.2003.12.006

at 100 °C for 24 h. The dried powders were then clacinated at 800 °C in air for 2 h in covered alumina crucibles. The calcined powders were further ball-milled for 6 h and granulated through 20 mesh screen and pressed at 13.8 MN/m$^2$ (2 ksi) into 10 mm disks. The disks were sintered at 1050 °C for 4 h. The disks were then pulverized into powder for crystal structural investigation.

Phase structure of the samples was examined using X-ray diffraction (XRD) and Raman Spectroscopy. XRD measurements were performed on a diffractometer with Cu Kα irradiation. Raman spectra analysis was conducted on the samples from 100 to 1000 cm$^{-1}$ using a Jobin-Yvon U1000 spectrometer and an argon laser operating at 488 nm and incident power of 20–30 mW. The microstructures of the surface of the disks were examined by scanning electron microscopy (SEM). Dielectric measurements at room temperature at 1 MHz were made using HP4194A impedance analyzer.

## 3. Results and discussion

Fig. 1 shows the XRD patterns of the samples. Cubic pyrochlore phase is the predominant phase in these samples.

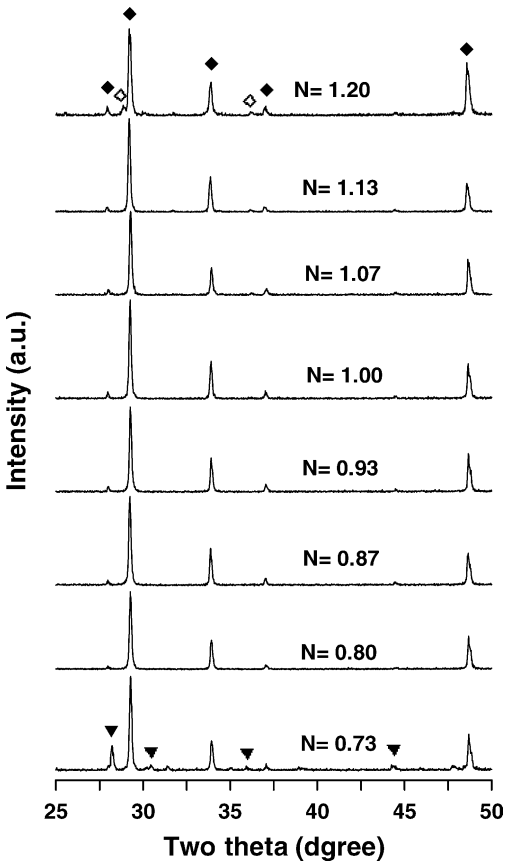


Fig. 1. X-ray diffraction patterns of the samples as a function of $N$ for $Bi_{1.5}Zn_NNb_{2.5-N}O_{8.5-1.5N}$. ◆: Cubic pyrochlore phase, ▼: $BiNbO_4$, ◇: ZnO.

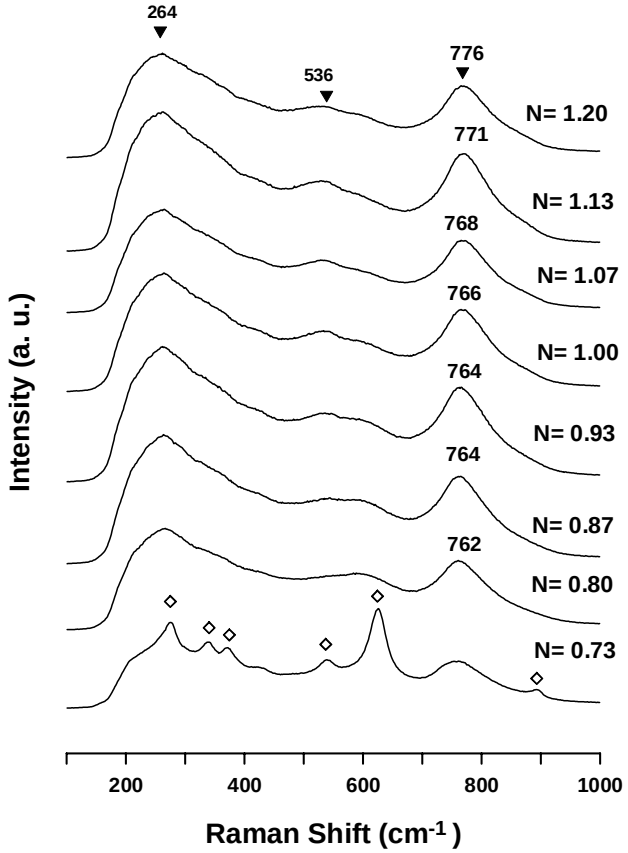


Fig. 2. Raman spectra of the samples as a function of $N$ with $Bi_{1.5}Zn_NNb_{2.5-N}O_{8.5-1.5N}$.

It was found that the sample with compositions in the range of $1.13 > N > 0.73$ shows nearly pure cubic pyrochlore phase. ZnO phase forms only for $N \geq 1.20$ and $BiNbO_4$ forms for $N \leq 0.73$. The evolution of the crystal structure was further examined using Raman spectroscopy as shown in Fig. 2. Three main bands at 264, 536, and 762 cm$^{-1}$

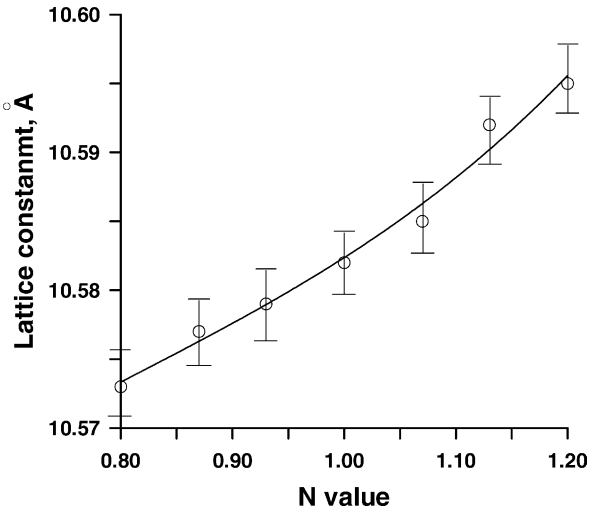


Fig. 3. Lattice constant as a function of $N$ with $Bi_{1.5}Zn_NNb_{2.5-N}O_{8.5-1.5N}$.

were observed in the Raman spectra. These bands have been assigned to the characteristic bands of cubic pyrochlore: 264 ($F_{2g}$), 536 ($E_g$), and 762 $cm^{-1}$ ($A_{1g}$) [13]. It was also found that the characteristic bands of $BiNbO_4$ were observed for $N = 0.73$. No other bands were observed in the samples with $N > 0.73$. The result of Raman spectra is in good agreement with the XRD analysis. Therefore, it can be concluded that single pyrochlore phase forms with $1.13 > N > 0.73$.

On the other hand, it was found that the frequency of the $A_{1g}$ vibration increased from 762 to 776 $cm^{-1}$ as the zinc content increased as seen in Fig. 2. A relationship between the frequency of the $A_{1g}$ vibrational band and B ion radius was reported earlier [14]. The larger the B ion radius (with the same A ion) the higher the observed $A_{1g}$ vibrational frequency, indicating that the force constant has increased. It was concluded that the ionic radius is an important factor for the magnitude of the force constant and thereby the position of the $A_{1g}$ vibrational band [15]. In our current investigation, the ionic radius of $Zn^{5+}$ (0.74 Å) is larger than that of $Nb^{5+}$ (0.64 Å). The increase in the $A_{1g}$ vibrational frequency when the Nb ion is substituted with Zn ion is thus attributed to the larger ionic radius of $Zn^{5+}$ than that of $Nb^{5+}$.

Fig. 3 shows the lattice constant of cubic pyrochlore phase versus the composition. It is found that the lattice constant

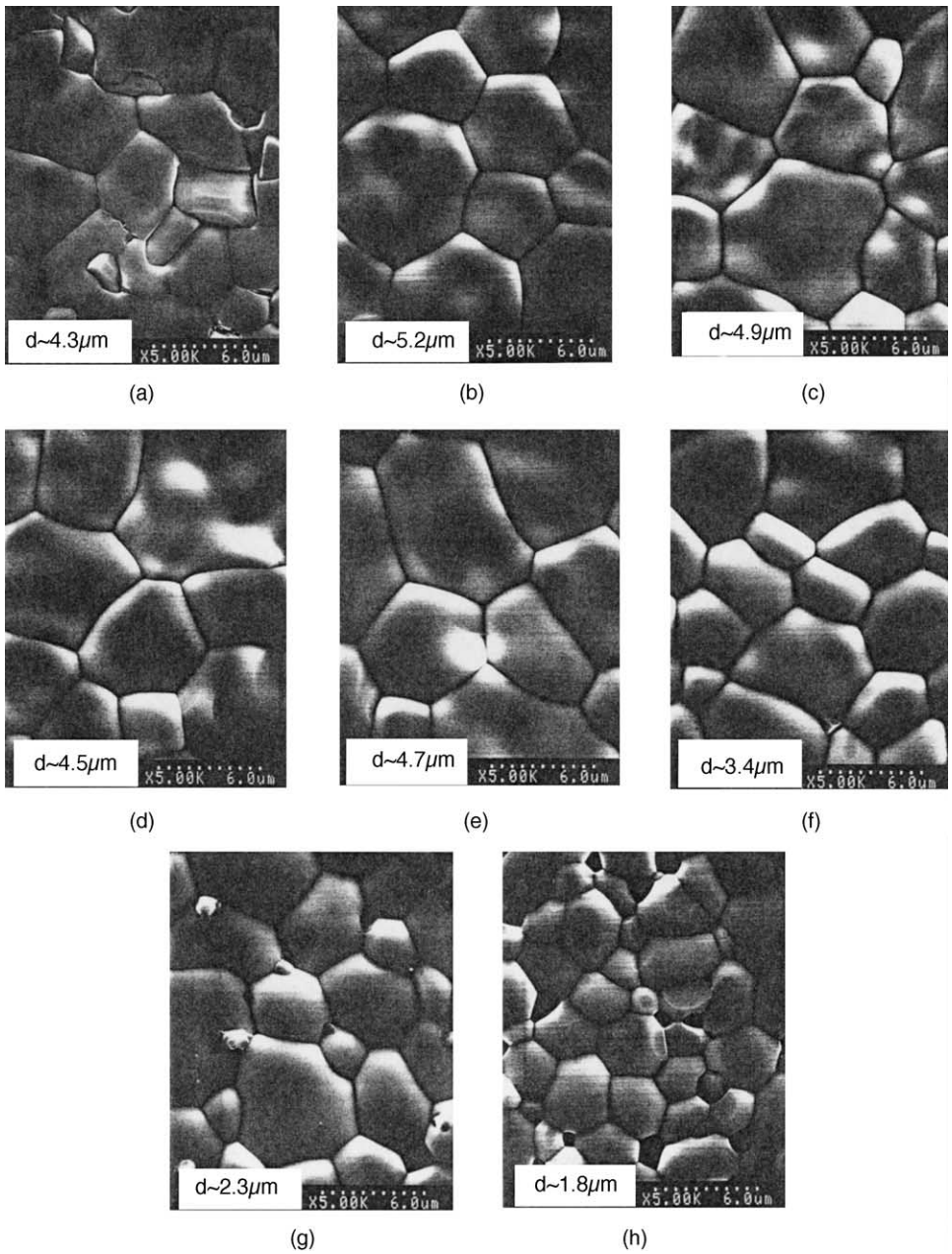


Fig. 4. SEM photographs on the surface of the sintered BZN disks. (a) $N = 1.20$, (b) $N = 1.13$, (c) $N = 1.07$, (d) $N = 1.00$, (e) $N = 0.93$, (f) $N = 0.87$, (g) $N = 0.80$, (h) $N = 0.73$.

increases with the increase of $N$ value. It is reasonable to explain the expansion in the lattice constant as the $Nb^{5+}$ is substituted with the larger $Zn^{2+}$ ion.

Fig. 4 shows the SEM photographs of the surface morphologies of the disk samples. It is found that the grain size of the samples slightly decreases with the increase of $N$ except for $N = 1.20$. The difference in the grain growth rate during sintering, which causes the variation in grain size, is attributed to the different diffusion rate of the ionic species. It was reported earlier that the diffusion mechanism underlying the conductivity of some of the pyrochlore oxides at high temperature is the oxygen ion-vacancy hopping mechanism [15]. The concentration of the oxygen vacancies seems to be the rate-controlling factor for grain growth.

Fig. 5 shows the dielectric constant of the sample versus the compositions of the specimens. The dielectric constant of the sample increases with the increase of $N$ value. Dielectric properties are usually proportional to the polarizability of the constituents. Since the polarizability of $Zn^{2+}$ (0.71) is larger than that of $Nb^{5+}$ (0.61), the dielectric constant increases as the $Nb^{5+}$ is substituted with $Zn^{2+}$. Fig. 6 shows the dielectric loss of the samples versus the compositions of the specimens. The dielectric loss of the samples increases with the increase of $N$ value. The dielectric loss is known to be related to the electrical conducting mechanisms. Hopping of oxygen ion has been suggested to be the major mechanism of the conducting mechanism of pyrochlore oxides [15]. The higher concentration of the defects in the samples as suggested results in higher dielectric loss.

Since the characteristics of the samples possibly correspond to the states of the defects, it would be necessary to analyze the characteristics of the defects theoretically. The formation of the defects due to nonstoichiometric composition is described by the following model, which uses the Kroger–Vink notation [16]. The defect model is based on the seven species: $Bi_A^{\times}$, $Zn_A^{\bullet}$ at A site (16c), $Nb_B^{\bullet}$, $Zn_B''$ at

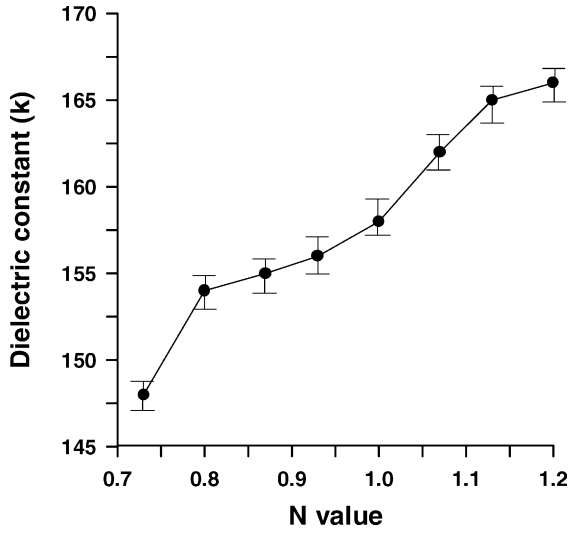


Fig. 5. Dielectric constants of the samples as a function of $N$ value.

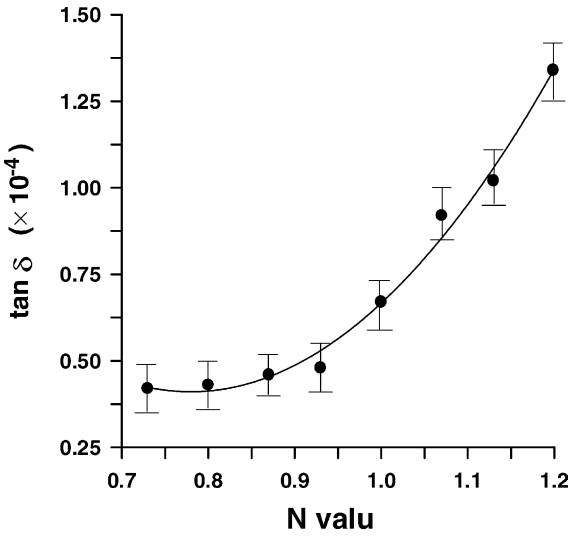


Fig. 6. Dielectric loss of the samples as a function of $N$ value.

B site (16d), $V_O^{\bullet\bullet}$, $O_O^{\times}$ at oxygen sites (48f, 8a), and $O_i''$ at oxygen site (8b). It is assumed that the model is valid for an oxygen partial pressure domain, where electronic defects (electron and holes) and reduced cations can be neglected. It is assumed that Bismuth ions ($Bi^{3+}$) resides only on the A sites, and niobium ions ($Nb^{5+}$) only on the B sites. Therefore, the following equations describing the interaction between the defect species are obtained based on the formula $(Bi_{1.5}Zn_{0.5})(Zn_{N-0.5}Nb_{2.5-N})O_{8.5-1.5N}$.

### 3.1. A site balance

The reference charge is 3+ for the A site. Therefore, the occupation of $Zn^{2+}$ ion at the A site would create oxygen vacancies due to the electron compensation.

$$3Bi_2O_3 + 2ZnO \leftrightarrow 6Bi_A^{\times} + 2Zn_A^{\bullet} + V_O^{\bullet\bullet} + 11O_O^{\times} \quad (1)$$

$$[Bi_A^{\times}] + [Zn_A^{\bullet}] = 2 \quad (2)$$

$$[V_O^{\bullet}]_A = \tfrac{1}{2}[Zn_A^{\bullet}] = 0.25 \quad (3)$$

Since the fraction of $Bi_2O_3$ is kept constant, the concentration of the oxygen vacancy from the A site balance is constant.

### 3.2. B site balance

The reference charge is 4+ for the B site. When $N$ equals to 1.167, the average charge of the ions is 4+. Two $Nb^{5+}$ ions at B site would create an oxygen interstitial whereas an $Zn^{2+}$ ion at B site would create an oxygen vacancy. The defect model must therefore include a chemical equilibrium involving all these species, i.e.

$$\tfrac{n}{2}Nb_2O_5 + (2-n)ZnO \leftrightarrow nNb_B^{\bullet} + (2-n)Zn_B'' + \tfrac{n}{2}O_i'' + (2-n)V_O^{\bullet\bullet} + (2+n)O_O^{\times} \quad (4)$$

where $n$=2.5−$N$

$$[Nb_B^{\bullet}] + [Zn_B''] = 2 \quad (5)$$

Electroneutrality condition:

$$[Nb_B^{\bullet}] + 2[V_O^{\bullet\bullet}]_A + [V_O^{\bullet\bullet}]_B = [Zn_B''] + [Zn_A'] + 2[O_i''] \quad (6)$$

The substitution of Nb with Zn at B site is assumed to provoke disorder on the cation distribution. Oxygen ions are also redistributed between the "normal" sites in a pyrochlore structure and the vacant 8b position. Boundary conditions are set based on the stoichiometric consideration:

(1) When $N$ equals to unity, the charge of the ions just balance to fit the exact pyrochlore phase. The overall defects in the structure should be zero: $[V_O^{\bullet\bullet}]_A + [V_O^{\bullet\bullet}]_B = [O_i'']$
(2) When $N$ equals to 1.167, the charge of the ions in the B site just balance to fit the 4+ charge. The concentration of oxygen vacancy equals to that of interstitial oxygen: $[V_O^{\bullet\bullet}]_B = [O_i'']$

Fig. 7 shows the results of the concentration of the defects based on the defect model. It has been hypothesized that seven oxygen ions distributed on eight sites per chemical formula of $A_2B_2O_7$ based on the statistical disorder [17]. It can be postulated that the pyrochlore defect model can be described as a case of a disordered fluorite "$A_2B_2O_7$" = $(A/B)O_{1.75}$, in which seven oxygen ions are distributed on eight 8b sites. This indicates that the complete disorder structure of pyrochlore structure has $[O_i''] = 7/8$ per unit formula. When $[O_i''] > 7/8 \sim 0.875$, the structure of pyrochlore becomes unstable. This is evidenced by the formation of the second phase, $BiNbO_4$, when $N$ is smaller than 0.8, at which $[O_i''] = 0.825$ as shown in Fig. 7.

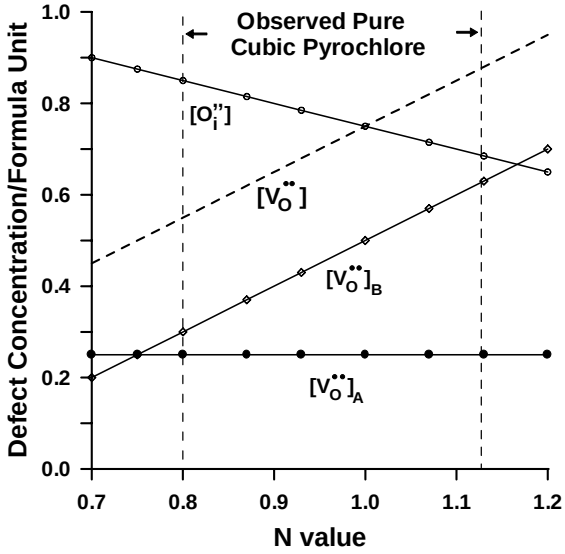


Fig. 7. Concentration of defect species in the $Bi_{1.5}Zn_NNb_{2.5-N}O_{8.5-1.5N}$ at fixed oxygen partial pressure based on the defect model. The dash line represents the amount of overall defects ($[V_O^{\bullet\bullet}] = [V_O^{\bullet\bullet}]_A + [V_O^{\bullet\bullet}]_B$).

It has been found that cation and/or anion vacancies in the A site network do not significantly reduce the stability of the lattice [18]. Most defect pyrochlores have oxygen vacancies on the 8a site, although some are also nonstoichiometric with respect to the A-type cations. However, if the sites at 8a are all vacant, the structure will more likely be the perovskite structure $A_2B_2O_6$ without the consideration of the oxygen interstitials. Adoption of the pyrochlore structure by an $A_2B_2O_6$ compound would introduce an additional 1/8 of oxygen vacancies. If the oxygen vacancies distributed only on the 8a sites, seven oxygen vacancies would distribute on the eight 8a sites. This indicates that the cubic pyrochlore structure would be unstable when the total oxygen vacancies $[V_O^{\bullet\bullet}] = [V_O^{\bullet\bullet}]_A + [V_O^{\bullet\bullet}]_B \geq 7/8 \sim 0.875$. This is evidenced by the formation of the second phase, ZnO, when $N$ is higher than 1.13, at which $[V_O^{\bullet}] = 0.875$ as shown in Fig. 7.

The composition region for the formation of single pyrochlore phase, $0.8 \leq N \leq 1.13$, has been marked by vertical dashed lines in Fig. 7. The model, therefore, reasonably reveals the defect chemistry of the pyrochlores. The dielectric loss of the samples seems to be corresponding to the concentration of oxygen vacancies. The dielectric loss of the samples increases as the concentration of oxygen vacancies increases (Figs. 6 and 7). The concentration of oxygen defects would also affect the grain growth rate during sintering. The grain size of the samples increases with the increase of the concentration of oxygen vacancies and the decrease of the concentration of oxygen interstitials (Figs. 4 and 7). It has been reported that the conduction mechanism is p-type at 1000 °C in air for some pyrochlore oxides [14]. This indicates that the concentration of oxygen interstitial is the main factor for the diffusion process. The present defect model provides good agreement with the experimental characteristics of the cubic pyrochlores.

## 4. Summary

It was concluded that single pyrochlore phase forms with $1.13 \geq N \geq 0.8$ of the composition of $Bi_{1.5}Zn_NNb_{2.5-N}O_{8.5-1.5N}$ (with $N$ = 0.73 to 1.20) under 1050 °C heat treatment for 4 h. Lattice constant of cubic pyrochlore and dielectric constant of the samples increased with the increase of Zn content. The dielectric constant and dielectric loss of the samples increase with the increase of $N$ value. A model of the structural defects is proposed to explain the stabilization of the cubic pyrochlore structure. The limitation of composition for the formation of pure cubic pyrochlore phase is attributed to the distribution of oxygen interstitials and vacancies.

## Acknowledgements

Financial support of this research by National Science Council, Taiwan, ROC, under the grant NSC 89-2216-E-036-029 is gratefully acknowledged.

## References

[1] D.P. Cann, C.A. Randall, T.R. Shrout, Solid State Commun. 100 (1996) 529–534.
[2] D. Liu, Y. Liu, S.-Q. Huang, X. Yao, J. Am. Ceram. Soc. 76 (1993) 2129–2132.
[3] M.F. Yan, H.C. Ling, Mater. Chem. Phys. 44 (1996) 37–44.
[4] H.C. Ling, M.F. Yan, W.W. Rhodes, J. Mater. Res. 5 (1990) 1752–1762.
[5] X. Wang, H. Wang, X. Yao, J. Am. Ceram. Soc. 80 (1997) 2745–2748.
[6] M.A. Subramanian, G.V. Subba Rao, Prog. Solid State Chem. 15 (1983) 55–143.
[7] Y. Hu, C.-L. Huang, Mater. Chem. Phys. 72 (2001) 60–65.
[8] A. Mergen, W.E. Lee, Mater. Res. Bull. 32 (1997) 175–189.
[9] G. Jeanne, G. Desgardin, B. Raveau, Mater. Res. Bull. 9 (1974) 1321–1322.
[10] R.A. Beyerlein, H.S. Horowitz, J.M. Longo, J. Solid State Chem. 72 (1988) 2–8.
[11] J.A. Alonso, C. Cascales, I. Rasines, J. Pannetier, Phys. B 156/157 (1989) 107.
[12] B.J. Kennedy, J. Solid State Chem. 123 (1996) 14–20.
[13] H.C. Gupta, S. Brown, N. Rani, V.B. Gohel, J. Phys. Chem. Solids 63 (2002) 535–538.
[14] F.W. Poulsen, M. Glerup, P. Holtappels, Solid State Ionics 135 (2000) 595–602.
[15] P.J. Wilde, C.R.A. Catlow, Solid State Ionics 112 (1998) 173–183.
[16] F.A. Kroger, H.J. Vink, in: F. Seitz, D. Turnbull (Eds.), Solid State Physics, Academic Press, New York, 1956, pp. 307–435.
[17] J.H. Lee, M. Yashima, M. Kakihana, M. Yoshimura, J. Am. Ceram. Soc. 81 (1998) 894–1794.
[18] J. Pannetier, J. Phys. Chem. Solids 34 (1973) 583–587.